Phys Chem Minerals (2003) 30: 469–477
DOI 10.1007/s00269-003-0340-4

ORIGINAL PAPER

P. A. van Aken · S. Lauterbach

Strong magnetic linear dichroism in Fe L_{23} and O K electron energy-loss near-edge spectra of antiferromagnetic hematite α-Fe_2O_3

Received: 6 January 2003 / Accepted: 4 June 2003

Abstract We report strong magnetic linear dichroism (MLD) at the Fe L_{23} and O K edges of the antiferromagnetic compound hematite α-Fe_2 O_3 in high-resolution orientation- and temperature-dependent electron energy-loss spectroscopy (EELS). Large intensity differences of corresponding spectral features are observed when the Fe L_{23} and O K edges are measured with momentum transfer either parallel or perpendicular to the magnetization. The resultant difference spectra for the Fe L_{23} edges is consistent with the MLD observed in X-ray absorption spectroscopy. For the first time we have observed MLD at the O K edge, where the magnetic origin of this dichroism is demonstrated by temperature-dependent investigations across the Morin transition temperature $T_M =$ 263 K, at which the Fe electron spins, i.e. the magnetic moments, rotate by 90°. The O K edge MLD is interpreted in terms of superexchange between the spins of the Fe 3d and O 2p electrons through overlapping Fe 3d and O 2p orbitals. The experiments were performed in a transmission electron microscope (TEM), yielding information about the anisotropic electronic structure at nanoscale spatial resolution when operated with a focused electron probe. The effects of MLD at the Fe L_{23} edges on the determination of $Fe^{3+}/\Sigma Fe$ in hematite at submicrometre scale using different independent quantification methods are discussed.

Keywords Magnetic linear dichroism (MLD) · Electron energy-loss spectroscopy (EELS) · Energy-loss near-edge structure (ELNES) · Transmission electron microscopy (TEM) · Hematite · Ferrous/ferric ratios

P. A. van Aken (✉) · S. Lauterbach
Institut für Angewandte Geowissenschaften,
Fachgebiet Geomaterialwissenschaft,
Technische Universität Darmstadt,
Schnittspahnstr. 9, 64287 Darmstadt
e-mail: vanaken@geo.tu-darmstadt.de
Tel.: +49-6151-162180
Fax: +49-6151-164021

Introduction

Rock magnetism has fascinated geoscientists, since it is both a basic and an applied science in order to reproduce and understand the processes by which igneous rocks are magnetized in nature. The study of microstructural magnetism is, at present, possible by transmission electron microscopical techniques, where phase shifts produced by the magnetic vector potential in ferromagnetic samples can generate phase contrast which is used in Lorentz microscopy to determine the distribution of magnetization (e.g. Reimer 1993). Recent developments of spectroscopic techniques using high-intensity polarized photon beams from newest generation synchrotron radiation facilities enable access to magnetic properties by investigation of X-ray magnetic dichroism (e.g. Stöhr et al. 1998). If these experiments are combined with X-ray photoemission electron microscopy (XPEEM), high spatial resolution on the order of 20 nm can be obtained (Nolting et al. 2000), which thus allows the magnetic microstructure to be imaged.

X-ray absorption spectroscopy (XAS), a technique based on the absorption of photons, is a sensitive probe for the electronic structure with a specificity for element, site-symmetry and valency (van der Laan and Kirkman 1992). The specificity arises from the characteristic binding energies of the atomic core electrons. At the absorption thresholds of the elements, the spectra show strong resonances arising from transitions to unfilled valence states. In the case of light elements, like boron, carbon, oxygen and nitrogen, these states are unfilled molecular orbitals, while in the case of 3d transition metals, the states correspond to the unfilled valence band. Since the electronic dipole transitions are governed by the $\Delta l = \pm 1$ selection rule, light elements are studied using K edges (1s $\rightarrow$ p transitions), and 3d transition metals are best studied using L_{23} edges (2p $\rightarrow$ d(s) transitions).

In practice, XAS is carried out with polarized synchrotron radiation, where the polarization of the X-rays can be changed from left or right circular to linear.

Circularly polarized X-rays are particularly useful for the study of ferromagnets or ferrimagnets. In order to determine the difference in the number of *d* holes with up and down spin (the magnetic moment), the X-ray absorption process has to be measured spin-dependently. This is done by the use of right or left circularly polarized photons which transfer their angular momentum (photon spin) to the excited photoelectrons. Therefore, much attention has focused on magnetic circular dichroism (MCD), defined as the difference in absorption cross-section for left- and right-circular polarized X-rays, which is proportional to the expectation value of the local magnetic moment $\langle \vec{M} \rangle$. The foremost strength of X-ray magnetic circular dichroism spectroscopy, first suggested by Erskine and Stern (1975) and pioneered by Schütz and coworkers in both the near-edge (Schütz et al. 1987) and extended fine-structure regimes (Schütz et al. 1989), is its specificity for element and its capability to determine the sizes and directions of spin and orbital magnetic moments quantitatively as well as their anisotropies. Since MCD requires a net magnetization $\langle \vec{M} \rangle \neq 0$, it is zero for antiferromagnetic materials.

It is well known that linearly polarized X-rays can be used to probe the orientation of molecular orbitals (van der Laan et al. 1986, 1996; van der Laan and Thole 1991; Kuiper et al. 1993, Schofield et al. 1998). Hence, linearly polarized XAS can sense the charge anisotropy of the valence states involved in the core excitation process and can detect the number of valence holes in different directions of the atomic volume. In most cases, the anisotropy of the charge in the atomic volume is caused by crystal-field interaction and is due to an anisotropy in the bonding. This so-called natural linear dichroism can be present in the absence of a magnetic exchange field. For magnetic materials, however, the alignment of the local atomic spins can also cause an anisotropy in the charge through the spin-orbit coupling. For example, in a cubic material the charge is highly isotropic in the atomic sphere, but in the presence of a magnetic interaction it shows a small ellipse-like distortion about the magnetic direction. This charge anisotropy leads to an asymmetry of the X-ray absorption signal. Consequently, magnetic linear dichroism (MLD) spectroscopy (van der Laan et al. 1986, van der Laan and Thole 1991; Kuiper et al. 1993), defined as the difference in absorption cross section for incident electric fields polarized parallel and perpendicular to the magnetization in the material, provides a powerful tool in order to determine the direction of the magnetic axis in antiferromagnets. MLD depends on the average value of $\langle \vec{M}^2 \rangle$ of the ions in the solid (Thole and van der Laan 1985), and can therefore be strong in any system with collinear magnetic ordering, whether it be ferromagnetic or antiferromagnetic.

Electron energy-loss spectroscopy (EELS) measures the energy distribution of initially monoenergetic electron, after they have interacted with the ions in a solid. For small scattering vectors and close to the threshold, the transitions are governed by the electric dipole selection rules and, thus, the interpretation of EELS follows therefore similar lines as that of XAS (Egerton 1996). It has been well documented that for an excitation process the component waves are longitudinally polarized parallel to the direction of the momentum transfer $\vec{q} = \vec{k}_i - \vec{k}_f$, where the terms $\vec{k}_i$ and $\vec{k}_f$ denote the initial and final wave vectors of the high-energy electron. This means that linearly polarized measurements are feasible (e.g. van Aken et al. 1999), and with the control of the polarization direction relative to the magnetization $\vec{M}$ make the observation of MLD in EELS possible.

Hematite, α-Fe_2O_3, is an instructive example for studying MLD using EELS, since its crystal structure (Blake et al. 1966, Waychunas 1991 and references therein) and magnetic structure (e.g. Banerjee 1991 and references therein; Dunlop and Özdemir 1997 and references therein) is well known. Rhombohedral α-Fe_2O_3 (space group $R\bar{3}c$, lattice constants $a_0 = 0.5035$ nm and $c_0 = 1.3749$ nm) consists of hexagonal close-packed (001) layers of oxygen atoms with two thirds of the octahedral holes filled by Fe atoms. There are six formula units in the conventional hexagonal unit cell, combining to yield the uniaxial corundum structure in which the iron atoms are coordinated by six oxygen atoms with a slight deviation from octahedral symmetry with three short ($d_{\mathrm{Fe–O}} = 0.1943$ nm) and three long Fe–O bond lengths ($d_{\mathrm{Fe–O}} = 0.2115$ nm), respectively. The charge-transfer insulator hematite (Ma et al. 1993 and references therein) is an antiferromagnetic mineral below its Néel temperature $T_N = 948$ K (Banerjee 1991, Dunlop and Özdemir 1997). The corresponding magnetic structure (space group $R\bar{3}$) consists of antiferromagnetically coupled alternating (001) layers of spin up and spin down iron atoms (Banerjee 1991; Dunlop and Özdemir 1997), where two different modifications of this antiferromagnetic structure are observed: below the Morin temperature $T_M = 263$ K the Fe electron spins are perfectly aligned with the [001] hexagonal axis, implying that the net magnetization $\langle \vec{M} \rangle = 0$, while for $T_M < T < T_N$, they lie in the (001) basal planes. In the absence of an external magnetic field, α-Fe_2O_3 exhibits three antiferromagnetic domains, obtained by a $\pm$ 120° rotation of a single domain around the trigonal axis. Furthermore, in this temperature range a weak ferromagnetic moment at right angles to the average spin alignment axis is present due to a slight canting of the spins $\phi \approx 0.2°$, which is a weak non-collinearity of antiparallel magnetic moments (Dunlop and Özdemir 1997). Theoretical calculations (Sandratskii and Kübler 1996) have shown that spin-orbit coupling is responsible for this canted magnetic structure.

The empty electronic states of hematite have been studied experimentally by XAS at both the O *K* edge (de Groot et al. 1989; Ma et al. 1993; Mackrodt et al. 1999; Wu et al. 1997) and at the Fe L_{23} edges (Cressey et al. 1993; Crocombette et al. 1995; Thole and van der Laan 1988; van der Laan and Kirkman 1992) and EELS at the same edges (Colliex et al. 1991; Garvie et al. 1994; Krivanek and Paterson 1990; Paterson and Krivanek

1990; van Aken et al. 1998a,b). In this work, the Fe L_{23} and O K electron energy-loss near-edge structures (ELNES) of an α-Fe_2O_3 single crystal have been investigated by orientation- and temperature-dependent EELS. We concentrate here on EELS spectra with an angle between the incident beam direction $\vec{k}_i$ and crystallographic c-axis changing from 0° ($\vec{k}_i // \vec{c}$) to 90° ($\vec{k}_i \perp \vec{c}$). Since for $T < T_M$ and for $T > T_M$ the magnetization is $\vec{M} // \vec{c}$ and $\vec{M} \perp \vec{c}$, respectively, we are able to study the effect of momentum transfer $\vec{q}$ with respect to the orientation of $\vec{M}$ on the Fe L_{23} and O K edges and to observe MLD in EELS. Hematite, where the orientation of the magnetic moments flips by 90° across the Morin transition, provides a perfect model system to study MLD, since the observed changes at the Fe L_{23} and O K ELNES are due to the change of spin direction directly, without disturbing effects from structural anisotropy. The sign and magnitude of the observed effect at the Fe L_{23} edges are compared with the corresponding ones obtained in EELS (Yuan and Menon 1997; Menon and Yuan 1999) and in XAS (Kuiper et al. 1993) measurements on the same compound. Furthermore, the Fe L_{23} core-loss edges provide chemical information about the iron oxidation state, where the valence-specific multiplet structures can be used to determine $Fe^{3+}/\Sigma Fe$ (Garvie and Buseck 1998; van Aken et al 1998a; van Aken and Liebscher 2002). The effects of MLD at the Fe L_{23} edges on the determination of $Fe^{3+}/\Sigma Fe$ in hematite at submicrometre scale using different independent quantification methods are demonstrated. For the first time we have observed MLD at the O K edge, where the magnetic origin of this dichroism is demonstrated by temperature-dependent investigations across the Morin transition temperature.

Experimental

The sample used for EELS investigations was a natural single-crystal hematite (Tamnau collection, TU Darmstadt). Energy-dispersive microanalysis (EDX) and selected area electron diffraction revealed its pure α-Fe_2O_3 composition, since no other elements were detected within detection limits. Polished thin sections were prepared and then thinned to perforation by Ar ion-beam bombardment. To avoid structural damage during preparation, ion-beam thinning was carried out at an acceleration voltage of 3.0 kV using a Gatan Pips and a succeeding surface-cleaning procedure at a relatively low acceleration voltage of 1.5 kV using a Gatan Duomill.

O K- and Fe L_{23}-ELNES spectra were collected with a Gatan DigiPEELS 766 parallel electron spectrometer attached to a Philips CM12 TEM operating at 120 kV. Due to operating in an undersaturated mode, the energy spread of the LaB_6 cathode defined as full width at half maximum height of the zero-loss peak was 0.6 eV. Relatively large sample areas ($Ø \approx 0.5$ µm in diameter) at low total probe current ($I_p \approx 1$ nA) were investigated, resulting in a low electron current density of $j \approx 3 \times 10^4$ $e^-(nm^2\ s)^{-1}$. The sample thickness z, as estimated from the low-loss spectra, was approximately 50 nm for different areas leading to an analyzed volume of about $V = \pi \cdot (Ø/2)^2\ z \approx 0.01\ \mu m^3$. Selected area electron diffraction (SAED) patterns were used to precisely orient the sample, e.g. with the incoming electron beam parallel to the [001] hexagonal axis. In order to perform temperature-dependent measurements, samples could be cooled down far below the Morin transition temperature (T_M = 263 K) to ca. 110 K with a Gatan liquid nitrogen cooling stage.

All spectra were collected in diffraction mode using a 2-mm PEELS aperture at small convergence α = 2.2 mrad and collection $\beta = 3.3$ mrad semiangles (Fig. 1). The measurements were performed with an energy dispersion of 0.1 eV/channel and integration times of $t = 5$ s to 10 s per read out. Further improvements to the signal-to-noise ratio were achieved by aligning and summing many (60 to 80) similar spectra. No sign of radiation damage was observed. Since the EELS spectrum can be described by an integration over convergence and acceptance angles, α and β exert an important control on the contributions with momentum transfer $\vec{q}$ from different directions (Menon and Yuan 1998). Thus, the resulting EELS spectrum always contains a range of $\vec{q}$ vectors. If $\vec{q}$ is decomposed into a component parallel to $\vec{k}_i$ ($q_{//}$) and one that is perpendicular to $\vec{k}_i$($q_\perp$), the dichroic information can still be obtained by collecting two different spectra containing varying weighting of the contributions from the two $\vec{q}$ components (Yuan and Menon 1997, Menon and Yuan 1999). The characteristic scattering angle θ_E is determined by the energy-loss ΔE and the energy of the incident electron $E_0 = 120$ keV (Egerton 1996), yielding $\theta_E = 2.44$ mrad for ΔE = 530 eV (O K edge) and $\theta_E = 3.27$ mrad for $\Delta E = 710$ eV (Fe L_3 edge). φ is the angle between the incident beam direction and the c-axis of the crystal (Fig. 1). The parallel weighting fraction ω is calculated using Eqs (9a–c) and (10) from Menon and Yuan (1998) and is a function of the angles α, β, θ_E and φ. Based on the calculated data presented in Fig. 2, we estimate that in our experimental O K- and Fe L_3-edge spectra, the contributions with momentum transfer parallel to the incident beam are about 60 and 70%, respectively.

Data reduction included the correction for dark current and channel-to-channel gain variation, the subtraction of an inverse power law background, and the removal of plural scattering contributions by the Fourier-ratio technique for which the low-loss region including the zero-loss peak and the Fe $L_{2,3}$ and O K edges were collected under the same experimental conditions from the same sample region (Egerton 1996). In order to evaluate the effects of linear dichroism on the temperature and/or tilt-angle-dependent O K and Fe L_3 edges, the spectra have been normalized to their integral intensities in the range 520 to 550 eV and 700 to 730 eV, respectively.

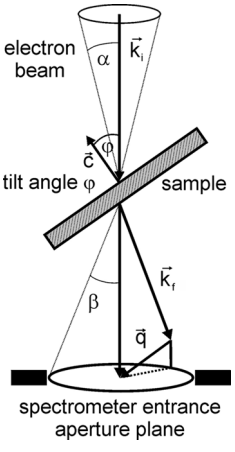

Fig. 1 Scattering geometry for the EELS experiments. The scattering vector $\vec{q}$ is the difference vector $\vec{q} = \vec{k}_i - \vec{k}_f$, where $\vec{k}_i$ and $\vec{k}_f$ are the initial and final wave vectors of the high-energy electron. The projection of $\vec{q}$ parallel and perpendicular to $\vec{k}_i$ are plotted by the *solid* and *dotted line*, respectively

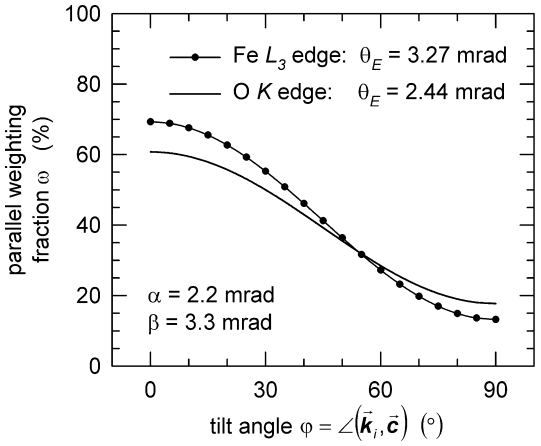

Fig. 2 Parallel weighting fraction ω as a function of tilt angle φ between the incident electron beam direction $\vec{k}_i$ and the $\vec{c}$ axis for experimental conditions with convergence $\alpha = 2.2$ mrad and collection $\beta = 3.3$ mrad semiangles: Fe L_3 edge (–•–•–) with $\theta_E = 3.27$ mrad, O K edge (——) with $\theta_E = 2.44$ mrad

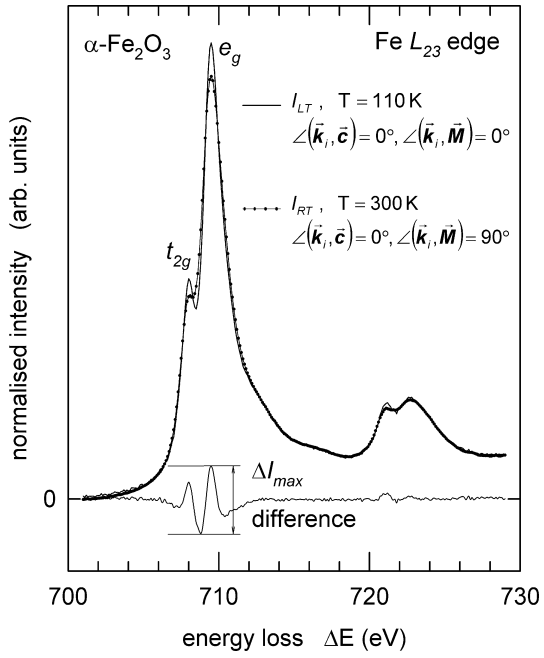

Fig. 3 Fe L_{23} edges of α-Fe_2O_3 with incident beam direction parallel $\vec{k}_i$ to the $\vec{c}$ axis at room temperature with $\angle(\vec{k}_i, \vec{M}) = 90°$ (–•–•–) and below the Morin transition temperature with $\angle(\vec{k}_i, \vec{M}) = 0°$ (——). The difference between both spectra is plotted on the same scale. Transitions from $2p$ into t_{2g} and e_g levels are indicated

Results and discussion

Fe L_{23} energy-loss near-edge structure

The Fe L_{23} edges are characterized by sharp maxima at the near-edge region, which are known as white lines. Although transitions from the Fe $2p$ to $3d$ and $4s$ symmetry orbitals are allowed by the selection rule of dipole transition, the probability of transition to the s orbitals is much lower and the Fe L_{23} spectra are dominated by excitation to Fe $3d$ orbitals. The spin-orbit interaction of the $2p$ core hole splits the Fe L_3 ($2p_{3/2}$) and L_2 ($2p_{1/2}$) edges by about 13 eV, and p–d and d–d Coulomb and exchange interactions causes the multiplet structures within the edges. The L_3 and L_2 white-line intensities are related to the unoccupied states in the $3d$ bands (van der Laan and Kirkman 1992).

For hematite with iron in the high-spin state, the atomic state changes from the $2p^6 3d^5$ Fe ground state to the $2p^5 3d^6$ final state after the excitation of a $2p$ core electron. α-Fe_2O_3 has a characteristic Fe L_3-edge-shape with a prepeak at 708.0 eV leading the main L_3 peak at 709.5 eV as in many other $^{[6]}Fe^{3+}$-containing minerals (e.g. van Aken and Liebscher 2002). The peaks have been assigned to $2p \rightarrow 3d$ transitions into low-energy t_{2g} and high-energy e_g orbitals using a simple crystal-field model (Krishnan 1990). In Fig. 3, two Fe L_{23} spectra (I_{LT}, I_{RT}) are displayed, acquired at small convergence $\alpha = 2.2$ mrad and collection $\beta = 3.3$ mrad semiangles (ca. 70% contribution from $\boldsymbol{q}_{//}$ components, cf. Fig. 2), and demonstrating the magnetic origin of the dichroism in α-Fe_2O_3. The spectra were measured with the incident beam parallel to the c-axis ($\vec{k}_i // \vec{c}$, $\varphi = 0°$) at low temperature ($T = 110$ K) below the Morin transition temperature T_M, where $\vec{M} // \vec{c}$, and at room temperature ($T = 300$ K) above T_M, where $\vec{M} \perp \vec{c}$. After background subtraction and removal of multiple scattering contributions, the Fe L_{23}-edge spectra have been aligned and normalized to their integral intensities between 700 and 730 eV. If we define the angle between $\vec{M}$ and $\vec{c}$ as φ^*, the normalized intensity distribution may be denoted for $T = 110$ K as I_{LT} and for $T = 300$ K as I_{RT}, and can be expressed in terms of contributions parallel and perpendicular to $\vec{M}$ as a function of the parallel weighting fraction ω as:

$$I_{LT}(\varphi^* = 0°) = \omega \cdot I_{//\vec{M}} + (1-\omega) \cdot I_{\perp\vec{M}} \quad \text{for } T < T_M \tag{1a}$$

$$I_{RT}(\varphi^* = 90°) = \omega \cdot I_{\perp\vec{M}} + (1-\omega) \cdot I_{//\vec{M}} \quad \text{for } T > T_M \tag{1b}$$

Here, $I_{//\vec{M}}$ and $I_{\text{perp}\vec{M}}$ are the intensities for incident field polarizations parallel and perpendicular to the magnetization $\vec{M}$, respectively. The difference spectrum is then calculated to

$$\begin{aligned} \Delta I &= I_{LT}(\varphi^* = 0°) - I_{RT}(\varphi^* = 90°) \\ &= (2 \cdot \omega - 1) \cdot (I_{//\vec{M}} - I_{\perp\vec{M}}) \ , \end{aligned} \tag{2}$$

which is proportional to the MLD $\left(I_{//\vec{M}} - I_{\perp\vec{M}}\right)$ for the system. The processed difference spectrum is also shown in Fig. 3. For obtaining the dichroic signal, the maximum at the Fe L_3 edge of the difference curve $\Delta I_{\max} = (I_{LT} - I_{RT})_{\max}$ and the maximum of the summed spectra $(I_{LT} + I_{RT})_{\max}$ are determined, and the normalized linear dichroic signal (LD) is calculated to:

$$LD = \frac{[I_{LT}(\varphi^* = 0°) - I_{RT}(\varphi^* = 90°)]_{\max}}{[I_{LT}(\varphi^* = 0°) + I_{RT}(\varphi^* = 90°)]_{\max}}. \quad (3)$$

The normalized dichroic signal yields ca. $LD \approx 8\%$ at the Fe L_3 edge of the acquired spectra presented in Fig. 3. Since the orientation of the sample during this temperature-dependent investigation is kept at $\vec{k}_i // \vec{c}$ ($\varphi = 0°$) and the scattering geometry is not modified (α, β = constant), the strong changes in the spectral shape of the Fe L_{23} edges are exclusively due to the spin–flip transition in α-Fe_2O_3. Rescaling of the dichroic signal obtained by EELS according to Eq. (4) should yield the linear dichroism observable by XAS:

$$\left.\frac{(I_{//\vec{M}} - I_{\perp\vec{M}})_{\max}}{(I_{//\vec{M}} + I_{\perp\vec{M}})_{\max}}\right|_{XAS} = \frac{1}{(2\cdot\omega - 1)} \cdot \left.\frac{(I_{LT} - I_{RT})_{\max}}{(I_{LT} + I_{RT})_{\max}}\right|_{\mathrm{EELS}} . \quad (4)$$

For the Fe L_3 edge, the parallel weighting fraction is $\omega \approx 0.7$ (cf. Fig. 2), and with $LD_{\mathrm{EELS}} \approx 8\%$ the rescaled LD has been calculated using Eq. (4), to 20%, which is in agreement with the observed maximum magnetic linear dichroism at the Fe L_3 edge in XAS (Kuiper et al. 1993). Closer inspection of the normalized Fe L_3-edge spectra in Fig. 3 yields that the low-energy t_{2g} peak of I_{RT} is lower in intensity than the t_{2g} peak of I_{LT}. The high-energy e_g peak of I_{RT} is also lower in intensity but is broader at the tails than the e_g peak of I_{LT}. As a consequence, the spectral shape of our difference spectrum (Fig. 3) differs from the data shown in Fig. 3 of Kuiper et al. (1993). Possible reasons for these diverging observations may be due to the presence of a longitudinal magnetic field in the pole piece of the objective lens of the TEM which is on the order of 1 T. Although this field is smaller than the local exchange field (Dunlop and Özdemir 1997), it might affect and alter the electronic structure and/or the excitation process. Furthermore, the EELS spectra were measured under non-kinematical conditions with the electron beam parallel to the [001] zone axis, where dynamical diffraction and scattering effects are strong and also could influence the Fe $2p \rightarrow 3d$ transitions. However, Yuan and Menon (1997) and Menon and Yuan (1999) investigated the linear dichroism of α-Fe_2O_3 by EELS studying the Fe L_{23} edges at room temperature at different convergence and collection angles. Our results resemble the difference spectrum from Yuan and Menon (1997) in both sign and size of the dichroic signal.

Next, we turn to the orientation dependence of the linear dichroism. Figure 4 shows four pairs of Fe L_3-edge spectra and the corresponding difference spectra, whereat the Fe L_3 ELNES, measured at different angles $\varphi^* = \angle(\vec{k}_i, \vec{M})$, are compared to the spectrum with $\varphi^* = 0°$. For the low-temperature spectra ($T = 110$ K), one observes an increase of the maximum difference signal $\Delta I_{\max}$ with increasing angle φ^*, where $\Delta I_{\max}$ is determined as defined in Fig. 3. The dichroic signal $\Delta I_{\max}$ further increases and reaches a maximum for the difference spectrum between I_{LT} ($\varphi^* = 0°$) and the room-temperature Fe L_3-edge spectrum with $\varphi^* = 90°$ measured

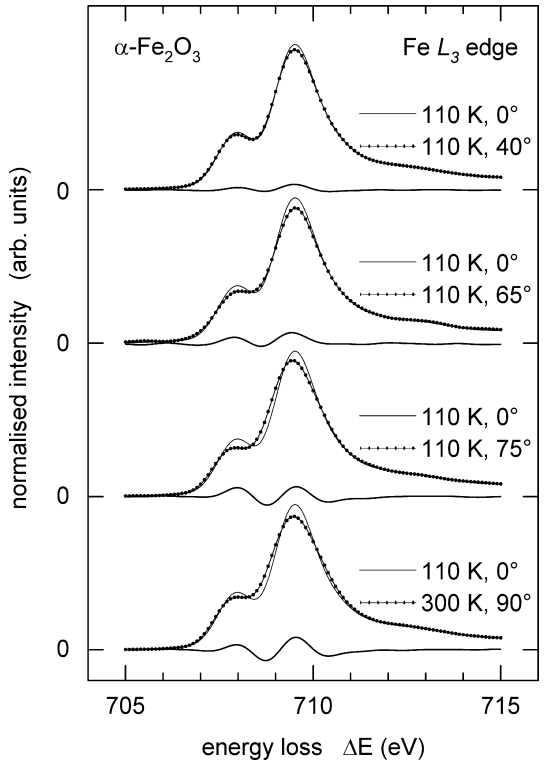

Fig. 4 Pairs of Fe L_3-ELNES spectra and corresponding differences plotted on the same scale of α-Fe_2O_3 with various angles ($\varphi^* = 0°$, 40°, 65°, 75°, 90°) between incident beam direction $\vec{k}_i$ and the magnetization $\vec{M}$. Some of the spectra have been shifted vertically for clarity

at $\vec{k}_i // \vec{c}$. Figure 5 presents the evolution of the normalized LD at the Fe L_3 edge calculated according to Eq. (3) as a function of the angle φ^* between $\vec{k}_i$ and $\vec{M}$. The data points follow within their estimated error bars a $k \sin^2(\varphi^*)$ function, which has been fitted including all data points. The fitting constant yields $k = 0.0756 \pm 0.0026$ with a goodness of fit of $r^2 = 0.96$. Since the maximum dichroitic signal $[I_{LT}(\varphi = 0°,\ \varphi^* = 0°) - I_{RT}(\varphi = 0°, \varphi^* = 90°)]$ is in accordance with the maximum of the $\sin^2(\varphi^*)$ function at $\varphi^* = 90°$, the observed variation of the normalized LD as a function of the tilt angle φ is basically due to changing the orientation of the magnetization in the $2p \rightarrow 3d$ excitation process. If the only contribution to the LD is of magnetic origin, one expects from the calculated parallel weighting fraction (cf. Fig. 2) a $\sin^2$ progression. This observation supports the results from Kuiper et al. (1993) that the contributions due to natural linear dichroism, in terms of crystal-field-induced dichroism because of slight deviations from octahedral symmetry, are definitely smaller than the contributions due to magnetic linear dichroism.

Subsequence, we focus on the effects of the observed MLD at the Fe L_{23} edges on the determination of $Fe^{3+}/\Sigma Fe$ in hematite. At present, quantification of ferrous/ferric ratios in minerals can be performed by detailed analysis of the valence-specific multiplet structures at the Fe L_{23} ELNES (van Aken et al. 1998a; Garvie and

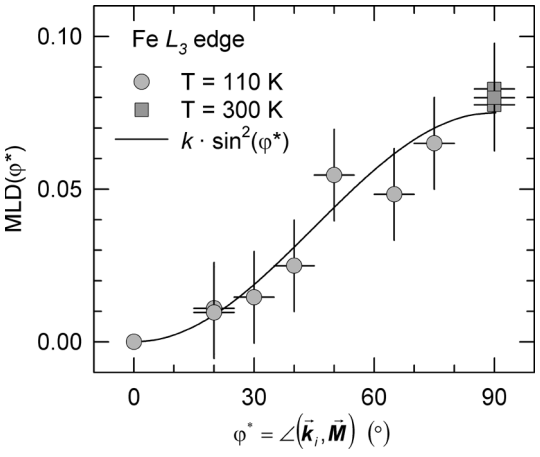

Fig. 5 Normalized magnitude of magnetic linear dichroism (MLD) at the Fe L_3-edge of α-Fe_2O_3 versus angle $\varphi^* = \angle(\vec{k}_i, \vec{M})$ between $\vec{k}_i$ and $\vec{M}$. The data points determined from low- and room-temperature Fe L_3 spectra are represented by *circles* and *squares*, respectively, and the fitted $k \cdot \sin^2(\varphi^*)$ function by the *solid line*

Buseck 1998; Calvert et al. 2001; van Aken and Liebscher 2002). Here, two different independent methods are applied for the $Fe^{3+}/\Sigma Fe$ quantification which has been described recently (van Aken and Liebscher 2002). (1) The modified integral intensity ratio of the Fe L_{23} white lines is determined by integration over two 2-eV-wide windows from which the $Fe^{3+}/\Sigma Fe$ ratio can be calculated using the universal curve. (2) A mathematical description of the Fe L_3 ELNES by fitting four Gaussian line profiles and an arctan function, where the relative integral intensity of the first peak is linearly related to $Fe^{3+}/\Sigma Fe$. For the first method the maximum absolute error in the $Fe^{3+}/\Sigma Fe$ quantification is about $\pm$ 0.04 and for the latter about $\pm$ 0.03. The effects of MLD at the Fe L_{23} edges is discussed representatively for the spectra I_{LT} ($\varphi = 0°$, $\varphi^* = 0°$) at $T < T_M$ and I_{RT} ($\varphi = 0°$, $\varphi^* = 90°$) at $T > T_M$, where maximum dichroism is observed.

The modified integral intensity ratio of the white lines has been determined to $I(L_3)/I(L_2)_{mod} = 8.95$ for I_{LT} and $I(L_3)/I(L_2)_{mod} = 9.70$ for I_{RT}, respectively. The $Fe^{3+}/\Sigma Fe$ ratios are then calculated with the use of the universal curve yielding $Fe^{3+}/\Sigma Fe(I_{LT}) = 0.93 \pm 0.04$ and $Fe^{3+}/\Sigma Fe(I_{RT}) = 1.00 \pm 0.04$. Similar results are obtained when the Fe L_3 ELNES spectra I_{LT} and I_{RT} are fitted using the mathematical description method. The normalized integral intensity of the first peak with respect to the total integral intensity of all four Gaussian lines yields $I_1/\Sigma I = 17.5\%$ for I_{LT} and $I_1/\Sigma I = 15.0\%$ for I_{RT}. From these values, the $Fe^{3+}/\Sigma Fe$ ratio is calculated using the linear relationship between $I_1/\Sigma I$ and $Fe^{3+}/\Sigma Fe$ which is shown in Fig. 6 of van Aken and Liebscher (2002) resulting in $Fe^{3+}/\Sigma Fe(I_{LT}) = 0.96 \pm 0.03$ and $Fe^{3+}/\Sigma Fe(I_{RT}) = 1.00 \pm 0.03$. For both evaluation procedures, the low-temperature Fe L_{23} spectra seem to show lower $Fe^{3+}/\Sigma Fe$ ratios. Since the sample orientation $[\varphi = \angle(\vec{k}_i, \vec{c}) = 0°]$ is the same for I_{LT} and I_{RT}, the reorientation of the magnetization $\vec{M}$ and the concomitant change of the spectral shape across the Morin transition is responsible for the differences in the calculated $Fe^{3+}/\Sigma Fe$ ratios. For the Fe L_3 edge and the scattering geometry used in our experimental setup, the contributions with momentum transfer parallel to the incident beam are about 70%. This means that at low temperature ($T < T_M$), the Fe L_3 ELNES consists of 70% of the signal parallel to $\vec{c}$ and consequently parallel to $\vec{M}(I_{//\vec{M}})$ and 30% perpendicular to $\vec{M}(I_{\perp\vec{M}})$. On the other hand, at temperatures above T_M, where $\vec{M} \perp \vec{c}$, 70% of the signal consists of $I_{\perp\vec{M}}$ and 30% of $I_{//\vec{M}}$. In the absence of any crystal-field-induced dichroism, as has been pointed out before, the isotropic Fe L_3-edge spectrum of hematite should be then given by $I_{iso} = \frac{1}{3} \cdot I_{//\vec{M}} + \frac{2}{3} \cdot I_{\perp\vec{M}}$. This situation resembles the room temperature spectrum with nearly identical weighting fractions for $I_{//\vec{M}}$ (1/3 vs. 30%) and $I_{\perp\vec{M}}$ (2/3 vs. 70%). Since the investigated hematite sample has pure α-Fe_2O_3 composition (see section Experimental), all iron cations are in the Fe^{3+} state. The analysis of the Fe L_{23} ELNES measured at room temperature yields $Fe^{3+}/\Sigma Fe = 1.00$, which confirms the hypothesis above that I_{RT} is equal to I_{iso}.

From these findings, it is obvious that MLD at the Fe L_{23} edges has an effect on the method of how the $Fe^{3+}/\Sigma Fe$ ratios are determined. Nevertheless, anisotropic effects and orientation dependence of Fe L_{23} ELNES spectra, like natural linear dichroism in brownmillerite (Gloter et al. 2000), can be minimized. Therefore, great care has to be taken in setting up the scattering geometry in terms of convergence and acceptance angles, and tilt angle between the principal axis and the incident beam direction. This topic has also been discussed extensively by several authors (Menon and Yuan 1998; van Aken and Liebscher 2002).

O *K* energy-loss near-edge structure

The O *K* edges result from an excitation of an O 1*s* core-level electron into empty states with O *p* symmetry. The near-edge structures arise from hybridization of the O 2*p* with Fe 3*d* and Fe 4*sp* states, which introduces O *p* character in unoccupied states of mainly Fe character (de Groot et al. 1989). Figure 6 shows the O *K*-edge spectra of α-Fe_2O_3 measured at $T = 110$ K (I_{LT}) and $T = 300$ K (I_{RT}). The orientation of the sample was kept at $\vec{k}_i // \vec{c}$. The spectra were acquired with $\alpha = 2.2$ mrad and $\beta = 3.3$ mrad, yielding ca. 60% contribution from $\boldsymbol{q}_{//}$ components (cf. Fig. 2). After the first data reduction, the spectra have been aligned and normalized to their integral intensities between 520 and 550 eV. One can divide the spectra in two regions: the first region is usually called the pre-peak region, where two components separated by 1.3 eV between 527 and 532 eV are observed. These features reflect transitions to anti-bonding O 2*p* states hybridized with Fe 3*d* states, and are interpreted as the $t_{2g} - e_g$ symmetry bands separated by the ligand-field splitting (de Groot et al. 1989). The

second region consists of a strong feature at about 540 eV with weaker shoulders at the low- and high-energy sides of the feature. The structures in this region are mainly due to covalent mixing of O 2*p* – Fe 4*s* and O 2*p*–Fe 4*p* states (de Groot et al. 1989).

The processed difference spectrum I_{LT}–I_{RT} is also shown in Fig. 6. In the first region, a normalized residual dichroic signal with a peak intensity of approximately $LD \approx 6\%$ of the acquired spectra is observed, whereas in the second region the low- and high-temperature O *K*-edge spectra agree perfectly in intensity distribution, resulting in a zero dichroic signal. The sign and spectral shape of the dichroic signal in the first region coincides with and matches the corresponding observed dichroic signal at the Fe L_3 edge (cf. Fig. 3). Since the only variable parameter was the temperature and concomitantly the direction of $\vec{M}$ with respect to $\vec{c}$, the changes in the spectral shape of the pre-edge feature are exclusively due to the reorientational Morin transition, without disturbing effects from structural anisotropy, demonstrating the magnetic origin of the observed linear dichroism at the O *K* edge in α-Fe_2O_3. To our knowledge, magnetic linear dichroism in O *K* EELS spectra has not been reported yet.

What is the mechanism of the observed MLD at the O *K* edge? In hematite, the magnetic structure consists of antiferromagnetically coupled alternating (001) layers of spin up and spin down Fe^{3+} ions (Banerjee 1991; Dunlop and Özdemir 1997), while in a given layer the spins are aligned ferromagnetically parallel to one another. The *d*-shell electrons of a Fe^{3+} ion (first iron layer) with one type of spin (up) orientation are coupled through the 2*p* electron orbit of an O^{2-} ion (intermediate oxygen layer) to the opposite type of spin orientation (down) of another Fe^{3+} ion (next-neighbouring iron layer). This phenomenon is called magnetic superexchange (Anderson 1959), because the coupling of the Fe 3*d* spins takes place via virtual excitations involving an intermediary O^{2-} ion. The hybridization between the Fe 3*d* and O 2*p* states can be described in terms of a molecular-orbital picture. As the e_g orbitals point towards the oxygen ligands, resulting in a strong overlap with the O 2*p* orbitals (forming σ bonds), the O 2*p*–Fe e_g hybridization is stronger than the O 2*p*–Fe t_{2g} one, since the t_{2g} orbitals are not directed towards the O 2*p* orbitals (forming π bonds). The Fe^{3+} ion has five *d* electrons. In an octahedral environment, two of these electrons singly occupy the Fe e_g orbitals, d_{z^2} and $d_{x^2-y^2}$, and three electrons occupy the Fe t_{2g} orbitals, d_{xy}, d_{xz} and d_{yz}, so that there are two e_g and three t_{2g} holes on iron. Due to Fe 3*d*–O 2*p* hybridization, the change of the density of hole states and its symmetry upon heating or cooling the sample above ($\vec{M} \perp \vec{c}$) or below ($\vec{M} // \vec{c}$) the Morin temperature is reflected not only in magnetic linear dichroism at the Fe L_{23} edges but also in MLD at the pre-edge feature of the O *K* edge. In an earlier paper, Mackrodt et al. (1999) described the possibility of using the O *K*-edge absorption spectra as a fingerprint of the magnetic structure. Their findings resulted from comparison of the experimental X-ray absorption O *K*-edge spectrum of hematite with a theoretical spectrum obtained from all-electron ab initio periodic Hartree-Fock calculations. Here, we present for the first time that O *K*-edge spectra are sensitive to temperature-dependent magnetic transitions in hematite.

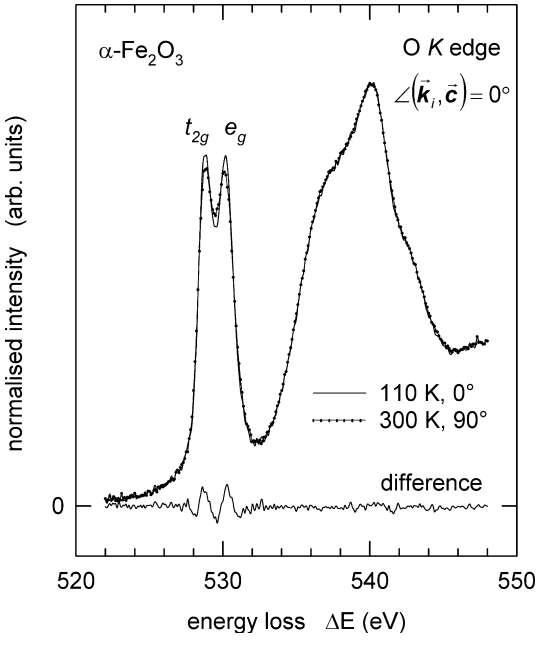

Fig. 6 O *K* edges of α-Fe_2O_3 measured at $\angle(\vec{k}_i, \vec{c}) = 0°$ and $T = 300$ K (–•–•–), where $\angle(\vec{k}_i, \vec{M}) = 90°$, and at $T = 110$ K (——), where $\angle(\vec{k}_i, \vec{M}) = 0°$. The difference between both spectra is plotted on the same scale. The t_{2g} and e_g features of the O *K*-edge pre-peak are indicated

Conclusions and summary

We have demonstrated by temperature- and orientation-dependent investigations of the Fe L_{23} and O *K* edges of hematite in electron energy-loss spectroscopy that magnetic linear dichroism can be strong in antiferromagnets. The reversal of the dichroism at the Morin temperature caused by the spin-flip transition in Fe_2O_3 convincingly shows that the observed dichroism is indeed mainly related to the orientation of the magnetization, and effects through natural linear dichroism are negligibly small. The magnitude of the dichroitic signal amounts to $LD_{\mathrm{EELS}} \approx 8\%$ of the maximum peak intensity at the Fe L_3 edge. The rescaled $LD_{\mathrm{EELS}}/(2\cdot\omega - 1)$ with respect to the parallel weighting fraction $\omega \approx 0.7$ is in perfect agreement with the observed maximum magnetic linear dichroism at the Fe L_3 edge in X-ray absorption spectroscopy $LD_{\mathrm{XAS}} \approx 20\%$. We have shown that MLD at the Fe L_{23} edges has an affect on the method of how $Fe^{3+}/\Sigma Fe$ ratios are determined. Therefore, great care has to be taken to minimize anisotropic effects and orientation dependencies of Fe L_{23} ELNES

spectra by using an experimental scattering geometry with which isotropic spectra can be measured.

For the first time, magnetic linear dichroism is observed at the O *K* pre-edge features of hematite. The sign and magnitude of the dichroitic signal at the O *K* edge agrees with the observed dichroism at the Fe L_3 edge. Since the antiferromagnetic order of iron ions is due to superexchange coupling involving intermediate oxygen ions and the O 2*p* orbitals are strongly hybridized with Fe 3*d* orbitals, the change of the unoccupied Fe 3*d* density of states due to the spin-flip transition is projected on the unoccupied O 2*p* density of states. Nevertheless, for an unambiguous interpretation of the observed MLD at the O *K* edge, the experimental spectra should be compared to theoretical calculations.

Acknowledgements We acknowledge financial support from the Deutsche Forschungsgemeinschaft (Grants AK 26/2-1,2). We are also grateful to P. Gebert for her thorough reading of and corrections to the manuscript.

References

Anderson PW (1959) New approach to the theory of superexchange interactions. Phys Rev 115: 2–13

Banerjee SK (1991) Magnetic properties of Fe–Ti oxides. In: (ed. Lindsley DH) Reviews in Mineralogy: Mineralogical Society of America. vol 25. Washinton, DC, pp 107–128

Blake RL, Hessevick RE, Zoltai T, Finger LW (1966) Refinement of the hematite structure. Am Mineral 51: 123–129

Calvert CC, Brydson R, Banks DA, Lloyd GE (2001) Quantification of Fe-oxidation state in mixed valence minerals: a geochemical application of EELS. Inst Phys Conf Ser 168: 251–254

Colliex C, Manoubi T, Ortiz C (1991) Electron-energy-loss-spectroscopy near-edge fine structures in the iron-oxygen system. Phys Rev (B) 44: 11402–11411

Cressey G, Henderson CMB, van der Laan G (1993) Use of L-edge X-ray absorption spectroscopy to characterise multiple valence states of 3d transition metals: a new probe for mineralogical and geochemical research. Phys Chem Miner 20: 111–119

Crocombette JP, Pollak M, Jollet F, Thromat N, Gautier-Soyer M (1995) X-ray-absorption spectroscopy at the Fe L_{23} threshold in iron oxides. Phys Rev (B) 52: 3143–3150

de Groot FMF, Grioni M, Fuggle JC, Ghijsen J, Sawatzky GA, Petersen H (1989) Oxygen 1*s* X-ray-absorption edges of transition-metal oxides. Phys Rev (B) 40: 5715–5723

Dunlop DJ, Özdemir Ö (1997) Rock magnetism. Fundamentals and frontiers. Cambridge University Press, Cambridge

Egerton RF (1996) Electron energy-loss spectroscopy in the electron microscope. 2nd ed. Plenum. New York

Erskine JL, Stern EA (1975) Calculation of the M_{23} magneto-optical absorption spectrum of ferromagnetic nickel. Phys Rev (B) 12, 5016–5024

Garvie LAJ, Buseck PR (1998) Ratios of ferrous to ferric iron from nanometre-sized areas in minerals. Nature 396: 667–670

Garvie LAJ, Craven AJ, Brydson R. (1994) Use of electron energy-loss near-edge fine structures in the study of minerals. Am Mineral 79: 411–425

Gloter A, Ingrin J, Bouchet D, Colliex C (2000) Composition and orientation dependence of the O *K* and Fe $L_{2,3}$ EELS fine structures in $Ca_2(Al_xFe_{1-x})_2O_5$. Phys Rev (B) 61: 2587–2594

Krishnan KM (1990) Iron L_{23}-near edge fine structure studies. Ultramicroscopy 32: 309–311

Krivanek OL, Paterson JH (1990) ELNES of 3*d* transition-metal oxides: I. Variations across the Periodic Table. Ultramicroscopy 32: 313–318

Kuiper P, Searle BG, Rudolf P, Tjeng LH, Chen CT (1993) X-ray magnetic dichroism of antiferromagnet Fe_2O_3: the orientation of magnetic moments observed by Fe 2*p* X-ray absorption spectroscopy. Phys Rev Lett 70: 1549–1552

Ma Y, Johnson PD, Wassdahl N, Guo J, Skytt P, Nordgren J, Kevan SD, Rubensson JE, Böske T, Eberhardt W (1993) Electronic structures of alpha-Fe_2O_3 and Fe_3O_4 from O *K*-edge absorption and emission spectroscopy. Phys Rev (B) 48: 2109–2111

Mackrodt WC, Jollet F, Gautier-Soyer M (1999) A first-principles Hartree–Fock interpretation of the X-ray oxygen *K*-edge spectrum of haematite (α-Fe_2O_3). Phil Mag (B) 79: 25–36

Menon NK, Yuan J (1998) Quantitative analysis of the effect of probe convergence on electron energy loss spectra of anisotropic materials. Ultramicroscopy 74: 83–94

Menon NK, Yuan J (1999) Towards atomic resolution EELS of anisotropic materials. Ultramicroscopy 78: 185–205

Nolting F, Scholl A, Stöhr J, Seo JW, Fompeyrine J, Siegwart H, Locquet JP, Anders S, Lüning J, Fullerton EE, Toney MF, Scheinfein MR, Padmore HA (2000) Direct observation of the alignment of ferromagnetic spins by antiferromagnetic spins. Nature 405: 767–769

Paterson JH, Krivanek OL (1990) ELNES of 3*d* transition-metal oxides: II. Variations with oxidation state and crystal structure. Ultramicroscopy 32: 319–325

Reimer L (1993) Transmission electron microscopy. Physics of image formation and microanalysis. Springer series in optical science, vol. 36, 3rd ed. Springer Berlin, Heidelberg New York eds.

Sandratskii LM, Kübler J (1996) First-principles LSDF study of weak ferromagnetism in Fe_2O_3. Europhys Lett 33: 447–452

Schofield PF, van der Laan G, Henderson CMB, Cressey G (1998) A single-crystal, linearly polarized Fe 2*p* X-ray absorption study of gillespite. Mineral Mag 62: 65–75

Schütz G, Wagner W, Wilhelm W, Kienle P, Zeller R, Frahm R, Materlik G (1987) Absorption of circularly polarized X-rays in iron. Phys Rev Lett 58: 737–740

Schütz G, Frahm R, Mautner P, Wienke R, Wagner W, Wilhelm W, Kienle P (1989) Spin-dependent extended X-ray-absorption fine structure: probing magnetic short-range order. Phys Rev Lett 62: 2620–2623

Stöhr J, Padmore HA, Anders S, Stammler T, Scheinfein MR (1998) Principles of X-ray magnetic dichroism spectromicroscopy. Surf Rev Lett 5: 1297–1308

Thole BT, van der Laan G (1988) Branching ratio in X-ray absorption spectroscopy. Phys Rev (B) 38: 3158–3171

Thole BT, van der Laan G, Sawatzky GA (1985) Strong magnetic dichroism predicted in the $M_{4,5}$ X-ray absorption spectra of magnetic rare-earth materials. Phys Rev Lett 55: 2086–2088

van Aken PA, Liebscher B, Styrsa VJ (1998a) Quantitative determination of iron oxidation states in minerals using Fe L_{23}-edge electron energy-loss near edge structure spectroscopy. Phys Chem Miner 25: 323–327

van Aken PA, Liebscher B, Styrsa VJ (1998b) Core level electron energy-loss spectra of minerals: pre-edge fine structures at the oxygen *K*-edge. Phys Chem Miner 25: 494–498

van Aken PA, Wu ZY, Langenhorst F, Seifert F (1999) ELNES spectroscopy and XANES calculations of the O *K* edge: orientation dependence and effetcs of protons in $Mg(OH)_2$. Phys Rev (B) 60: 3815–3820

van Aken PA, Liebscher B (2002) Quantification of ferrous/ferric ratios in minerals: new evaluation schemes of Fe L_{23} electron energy-loss near-edge spectra. Phys Chem Miner 29: 188–200

van der Laan G, Thole BT (1991) Strong magnetic X-ray dichroism in 2*p* absorption spectra of 3*d* transition-metal ions. Phys Rev (B) 43: 13401–13411

van der Laan G, Kirkman IW (1992) The 2*p* absorption spectra of 3*d* transition metal compounds in tetrahedral and octahedral symmetry. J Phys Condens Matter 4: 4189–4204

van der Laan G, Thole BT, Sawatzky GA, Goedkoop JB, Fuggle JC, Esteva JM, Karnatak R, Remeika JP, Dabkowska HA (1986) Experimental proof of magnetic X-ray dichroism. Phys Rev (B) 34: 6529–6531

van der Laan G, Schofield PF, Cressey G, Henderson CMB (1996) Natural linear dichroism at the Fe 2*p* absorption edge of gillespite. Chem Phys Lett 252: 272–276

Waychunas GA (1991) Crystal chemistry of oxides and oxyhydoxides, vol 25. (ed. Lindsley DH) Reviews in Mineralogy: Mineralogical Society of America, Washington, DC, pp 11–68

Wu ZY, Gota S, Jollet F, Pollak M, Gautier–Soyer M, Natoli CR (1997) Characterization of iron oxides by X-ray absorption at the oxygen K edge using a full multiple-scattering approach. Phys Rev (B) 55: 2570–2577

Yuan J, Menon NK (1997) Magnetic linear dichroism in electron energy-loss spectroscopy. J Appl Phys 81: 5087–5089